ELSEVIER

July 1996

Optical Materials 6 (1996) 55–61

OPTICAL Materials

Uncooled 4.2 μm light emitting diodes based on $InAs_{0.91}Sb_{0.09}$/GaSb grown by LPE

Y. Mao, A. Krier

Advanced Materials & Photonics Group, School of Physics & Chemistry, Lancaster University, Lancaster LA1 4YB, UK

Abstract

The report describes the epitaxial growth and fabrication of efficient room temperature $InAs_{0.91}Sb_{0.09}$ semiconductor light-emitting diodes operating in the infrared wavelength region at 4.2 μm. These devices have attracted much recent interest as viable infrared light sources for use in carbon dioxide detection. A study of the LPE growth of lattice matched $InAs_{1-x}Sb_x$ onto GaSb substrates from Sb-solution by the supercooled growth method is described. The electrical transport properties and photoluminescence are presented. The n–i–p-$InAs_{0.91}Sb_{0.09}$/P-GaSb light emitting diodes (LEDs) are studied and the quantum efficiency is discussed.

1. Introduction

The III–V ternary alloys $InAs_{1-x}Sb_x$ are potentially very important materials for the fabrication of light emitting diodes and detectors for middle-wavelength infrared applications due to their energy band gaps covering the range from 3–12 μm [1]. There is particular interest in the composition corresponding to $x = 0.09$ which is lattice matched to GaSb substrates and which has a room temperature energy gap near 4.2 μm, appropriate for the environmental/ecological monitoring of carbon dioxide using infrared optical techniques [2,3], since CO_2 has a strong absorption band at just this wavelength. Several groups have reported the successful growth of $InAs_{1-x}Sb_x$ epilayers by LPE [4–12], MBE [13–23] and MOCVD [24–27] and the fabrication of various devices [10,23,28–32]. In this paper, a study of some aspects of the various electro-optical characteristics of $InAs_{0.91}Sb_{0.09}$ materials and LEDs have been investigated.

2. Growth and characteristics of $InAs_{0.91}Sb_{0.09}$

Attempts to grow InAsSb onto GaSb substrates from In-rich melts result in rapid dissolution of the substrate followed by polycrystalline regrowth if conventional LPE techniques are used [5]. This is due to thermal instability of the GaSb substrate with respect to the In-rich InAsSb liquid [7]. The successful use of In-rich melts relies on the production of a state of extreme supersaturation at the melt-substrate interface, which involves maintaining a large temperature difference, usually larger than 20°C, between the melt and the substrate prior to their contact [5,10]. This results inevitably in rapid initial growth and is, therefore, not suitable for the production of thin epitaxial layers as required in the active region of heterostructure lasers for example. However, by using Sb-rich solution in the growth of $InAs_{1-x}Sb_x$ onto GaSb substrates, we can suppress the substrate erosion because the melt contains excess antimony in

PII S0925-3467(96)00011-0

this case [7]. By doing so, we can anticipate better device characteristics.

In order to obtain lattice matching, low surface etch-pit density and a smooth surface for the $InAs_{1-x}Sb_x$ epitaxial layers, the atomic fraction of indium χ^l_{In} in the melt should be as low as possible to provide a melt with enough antimony content to suppress erosion of the substrate. The melt with $\chi^l_{In} = 0.200$ and $\chi^l_{As} = 0.039$ has actually been confirmed as being the most suitable melt and a supercooling temperature of 2–3°C was the best condition found for LPE growth. The details of the epitaxial growth procedure have been described previously elsewhere [4].

The electron concentration in the lattice-matched undoped (n-type) $InAs_{0.91}Sb_{0.09}$ was measured to be $1–4 \times 10^{17}$ cm^{-3} by the (Van der Pauw) Hall technique in the temperature range 77–300 K, while the hole concentration in the zinc doped (p-type) $InAs_{0.91}Sb_{0.09}$ was found to increase strongly with the dopant atom fraction enabling heavy p-type doping at both 77 K and 300 K. The values of carrier mobility have been obtained as a function of temperature for both undoped (n-type) and zinc doped (p-type) $InAs_{0.91}Sb_{0.09}$. It was found that the mobilities in the undoped n-type $InAs_{0.91}Sb_{0.09}$ exhibit only a small variation in the temperature range from 77 K to 300 K, (i.e. 11 700 cm^2 V^{-1} s^{-1} at 77 K to 8800 cm^2 V^{-1} s^{-1} at 300 K) [33]. This behaviour is comparable to the electron mobility measurements for $InAs_{0.24}Sb_{0.76}$ MBE grown on InP [34].

The photoluminescence spectra at 78 K for a heavy Te doped n-type sample NA01 with 3.7×10^{-6} atomic fraction of Te, an undoped sample NA02 and two zinc doped samples PA101 and PA201 with 7.0×10^{-6} and 3.6×10^{-5} atomic fraction of zinc respectively are shown in Fig. 1. The carrier concentrations are 4×10^{19} cm^{-3} and 1×10^{17} cm^{-3} for the n-type samples and 1×10^{18} cm^{-3} and 6×10^{18} cm^{-3} for the p-type samples, respectively.

The PL peak energy for the doped n-type layer is 0.340 eV, which is 15 meV higher than that of the undoped layer. It seems that the electron transitions are from higher energy states in the conduction band due to a degenerate situation. The band filling from the band edge is about 15 meV according to the results of the PL measurements. The PL intensity at 78 K for the highly doped n-type sample is 40 times

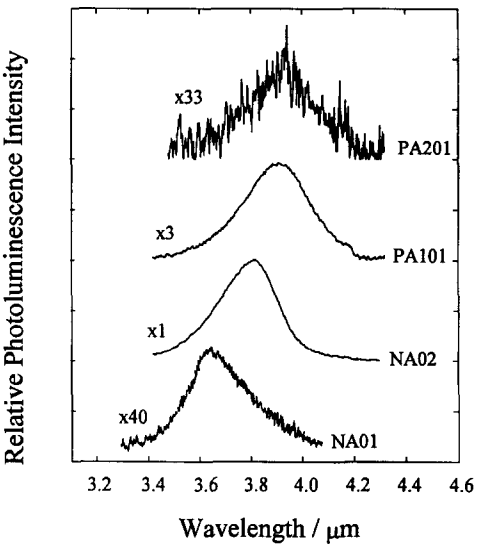

Fig. 1. The 78 K photoluminescence spectra from 4 μm thick Te doped n-type sample (NA01), 4 μm thick undoped n-type sample (NA02) and two 6 μm thick zinc doped p-type samples (PA101 and PA201).

lower than that of the undoped one. The PL peak positions of doped p-type samples being shifted to longer wavelength. These transitions are therefore from band to acceptor states. The PL intensities at 78 K for the doped p-type samples are 3 and 33 times lower than that of the undoped (n-type) sample, respectively. The very low quantum efficiency obtained from PL measurements at 78 K for these high carrier concentration n-type and p-type samples are due to Auger recombination becoming dominant. This can be explained from the plots of the calculated minority-carrier lifetimes against carrier concentration for both n- and p-type $InAs_{0.91}Sb_{0.09}$ at 78 K shown in Fig. 2, where τ_R, τ_{A1}, τ_{A7} and τ_{AS} represent the lifetimes for radiative recombination, CHCC, CHLH and CHSH Auger recombinations [35] respectively. It is apparent that the CHCC Auger recombination begins to become dominant for a carrier concentration of 10^{18} cm^{-3} ($n_0/n_i = 2 \times 10^{12}$) for n-type material as demonstrated by τ_{A1} which just begins to become larger than τ_R. As the carrier concentration increases, the Auger transition rate increases more strongly than the radiative rate because the Auger transition involves three carriers, while the radiative transition is a two carrier process. CHSH and CHLH Auger recombination becomes

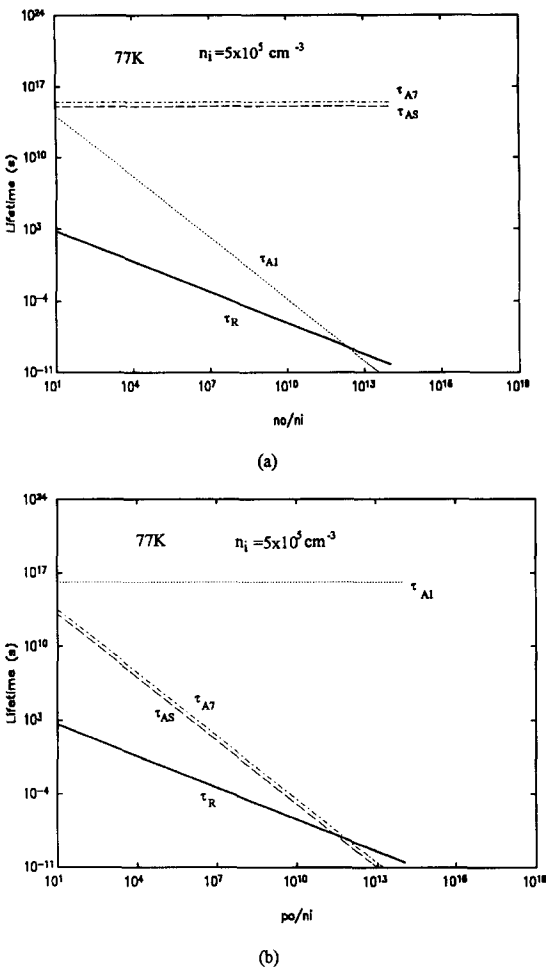

Fig. 2. Dependence of calculated carrier lifetime on normalized doping concentrations for $InAs_{0.90}Sb_{0.91}$ at 77 K for n-type (a) and p-type (b).

dominant at 78 K when the carrier concentration is larger than 10^{18} cm^{-3} for p-type $InAs_{0.90}Sb_{0.10}$ alloys, which leads to a weaker PL intensity being observed from sample PA201. The Auger effect is an important mechanism in determining the performance of LEDs made of these narrow gap semiconductors. In particular, the CHSH and CHLH processes dominate in heavily doped p-type materials when the band-gap energy (E_g) is comparable to or smaller than the spin–orbit splitting (Δ), which is true for $InAs_{0.90}Sb_{0.10}$ ($\Delta = 0.32$ eV), according to the analysis by Sugimura [36].

3. p–i–n $InAs_{0.91}Sb_{0.09}$ LEDs

Three layers p^+, i and n^+ of $InAs_{0.91}Sb_{0.09}$ were grown by LPE on (100) P-type GaSb substrates with a carrier concentration of $1-2 \times 10^{18}$ cm^{-3} obtained from MCP Wafer Technology Ltd. The n-type and p-type layers were doped to 10^{19} cm^{-3} and 10^{18} cm^{-3} by dopping with Te or Zn, while a carrier concentration of 10^{17} cm^{-3} was obtained for the unintentionally doped layer. The thicknesses were 3.3, 1.7 and 3.3 μm for the n^+, i and p^+ layers respectively. Circular mesa structures (area = 7.85×10^{-3} cm^2) were defined by standard photolithographic techniques. The LED chips were then metallised and mounted on To49 headers in the usual way.

Fig. 3 shows the uncorrected EL emission spectra obtained from one of the n–i–p-$InAs_{0.91}Sb_{0.09}$/P-GaSb diodes measured at 300 mA pulse drive current with 20% duty cycle in the temperature range of

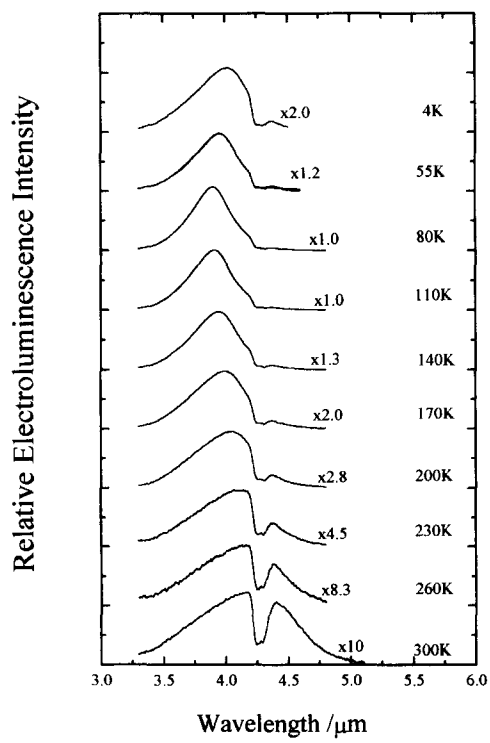

Fig. 3. The EL emission spectra measured at various temperatures for the n–i–p-$InAs_{0.91}Sb_{0.09}$/P-GaSb LED.

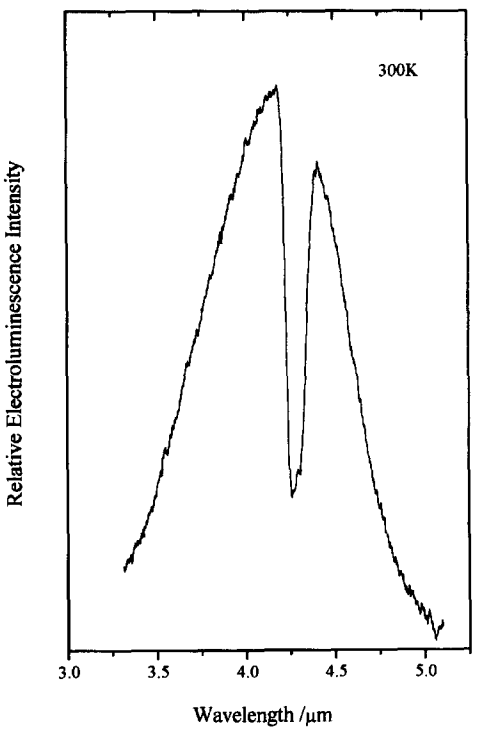

Fig. 4. Room temperature emission spectrum of an n–i–p-$InAs_{0.91}Sb_{0.09}$/P-GaSb LED measured in the laboratory atmosphere.

4–300 K. The peak emission wavelength is 4.02 μm at 4 K. The peak position first shifts slightly to shorter wavelength (blue shift) and the intensity increases with increasing temperature from 4–80 K, then as the temperature is increased above 80 K the peak shifts to longer wavelength (about 14 meV) and decreases in intensity by 10 times. The values of full width at half maximum (FWHM) decrease first from 40 meV (510 nm) to 32 meV (390 nm) as the temperature is increased from 4 to 80 K, then increase steadily to 68 meV (930 nm) as temperature increases to 300 K. A strong emission spectrum peaking at 4.21 μm (0.294 eV) was obtained at room temperature with a sharp dip at 4.27 μm which corresponds to CO_2 absorption at atmospheric concentration (0.03%) in the optical path of the detection system shown in Fig. 4. The results indicate that this InAsSb LED could form the basis of a portable solid-state CO_2 monitoring instrument.

By comparison of the EL spectra of this structure with the PL of n and p-type InAsSb as shown in Fig. 1 at 80 K, the EL peak position (0.318 eV) is similar to the PL peak position (0.317 eV) of the p-type layer and is smaller in energy than that of the undoped layer (0.325 eV). This indicates that the

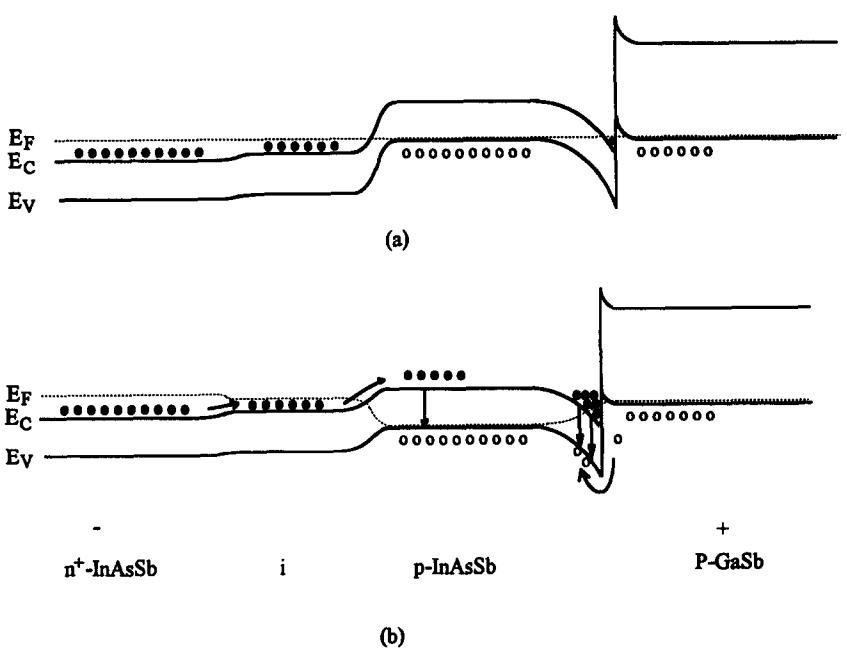

Fig. 5. The energy-band diagram of the n–i–p-$InAs_{0.91}Sb_{0.09}$/P-GaSb structure. (a) Zero bias; (b) forward bias.

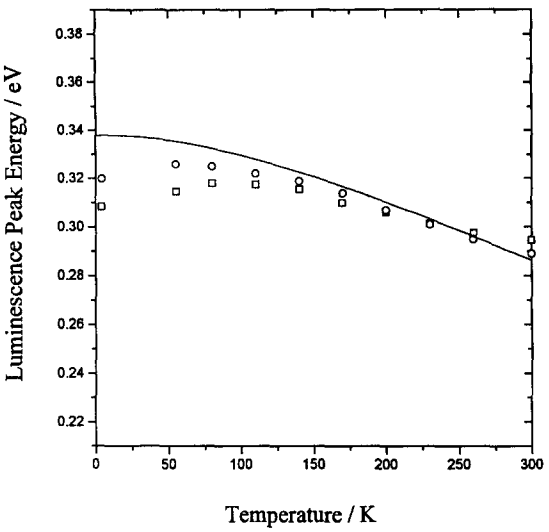

Fig. 6. Luminescence peak energy of EL and PL versus temperature. (□) EL of n–i–p-$InAs_{0.91}Sb_{0.09}$/P-GaSb; (○) PL of undoped n-type $InAs_{0.91}Sb_{0.09}$; (—) theoretically calculated temperature dependence of the energy gap for $InAs_{0.91}Sb_{0.09}$ alloy.

emission/recombination for the n–i–p-$InAs_{0.91}Sb_{0.09}$/P-GaSb LED structure is more likely to occur in the p-type layer rather than in the i layer. This also can be seen from analysis of the energy-band diagrams of the n–i–p-$InAs_{0.91}Sb_{0.09}$/P-GaSb structure which are shown in Fig. 5. Electrons and holes are injected into the p-type InAsSb region from the n-type InAsSb and p-type GaSb substrate respectively. The electrons are contained by the high barrier in the conduction band at the InAsSb–GaSb hetero-junction, and also the electrons are accumulated in the well on the narrow-band side (p-InAsSb) of the heterojunction, where the conductivity type reverses (inversion layer) because the band bending results in the fermi level being above the conduction band. Recombination of electrons and holes occurs both in the p-InAsSb region and at the p-P heterojunction shown in Fig. 5.

Fig. 6 shows the EL peak energy of the n–i–p-$InAs_{0.91}Sb_{0.09}$/P-GaSb diode versus temperature together with the PL results of an undoped $InAs_{0.91}Sb_{0.09}$ sample and the $InAs_{0.91}Sb_{0.09}$ energy gap from theoretical calculation [37] for comparison. The red shift at the low temperature in the EL of the n–i–p/P diode was mainly attributed to recombination via impurity levels and band edge transitions which is comparable to the PL results. But the EL peak energy of the n–i–p/P diode shifted more slowly than that of the PL as temperature rose to room temperature and the FWHM of the n–i–p/P EL was also slightly wider than that of the PL. This behaviour is perhaps associated with transitions involving interface states [2] at the p-P heterojunction.

The output optical power measured from the n–i–p/P LEDs (with no passivation or index-matching lens) was 2.9 μW with a current of 100 mA and 5% duty cycle at room temperature. The external quantum efficiency (η_{ext}) was derived to be about 10^{-4} at 300 K using the output optical power (P) and $\eta_{ext} = P/IV$ [38], where IV is the total electrical input power (I and V are the drive current and voltage). The η_{ext} for our LPE-grown, lattice-matched LEDs is much higher than for n-p-$InAs_{0.85}Sb_{0.15}$ LEDs grown on GaAs and Si substrates by MBE [31]. The external quantum efficiency of these latter LEDs reached a maximal value of the order of 10^{-4} only at 77 K and became poorer at room temperature, which is most likely due to the high density of dislocations in the structures.

An experimental determination of the internal quantum efficiency (η_{int}) defined as:

$$\eta_{int} = \frac{1}{1 + \tau_r/\tau_{nr}}, \tag{1}$$

where τ_r and τ_{nr} are the radiative and nonradiative lifetimes, respectively, is more difficult but can be obtained from external quantum efficiency measurements using the following relation $\eta_{ext} = \eta_i \eta_{opt} \eta_{int}$ [38], where η_i is a current injection efficiency which is defined as a ratio of the current due to minority carrier diffusion in the active region to the total current, and η_{opt} is an optical transmission efficiency or escape probability. The optical transmission efficiency is the fraction of the total generated radiation that is actually transmitted into the second medium (usually air) which is given by [39]:

$$\eta_{opt} = \frac{1}{4}\left(\frac{n_2}{n_1}\right)^2\left[1 - \left(\frac{n_1 - n_2}{n_1 + n_2}\right)^2\right], \tag{2}$$

where n_1 and n_2 are the refractive indices of the semiconductor and its surface medium respectively. The optical transmission efficiency (η_{opt}) was calcu-

Table 1
Comparison of the calculated and experimental internal quantum efficiency (η_{int}) for the $InAs_{0.91}$ $Sb_{0.09}$ epitaxial layers and LEDs

Temperature (K)	Calculated η_{int}		Experiment η_{int} LED
	Undoped n-type i-layer(10^{17} cm^{-3})	p-type (10^{18} cm^{-3})	
77	91%	9%	8%
300	2.6%	0.3%	0.8%

lated to be 0.013 for our LEDs. Then an estimate of the minimum internal quantum efficiency (η_{int}) can be obtained if the injection efficiency is assumed to be unity.

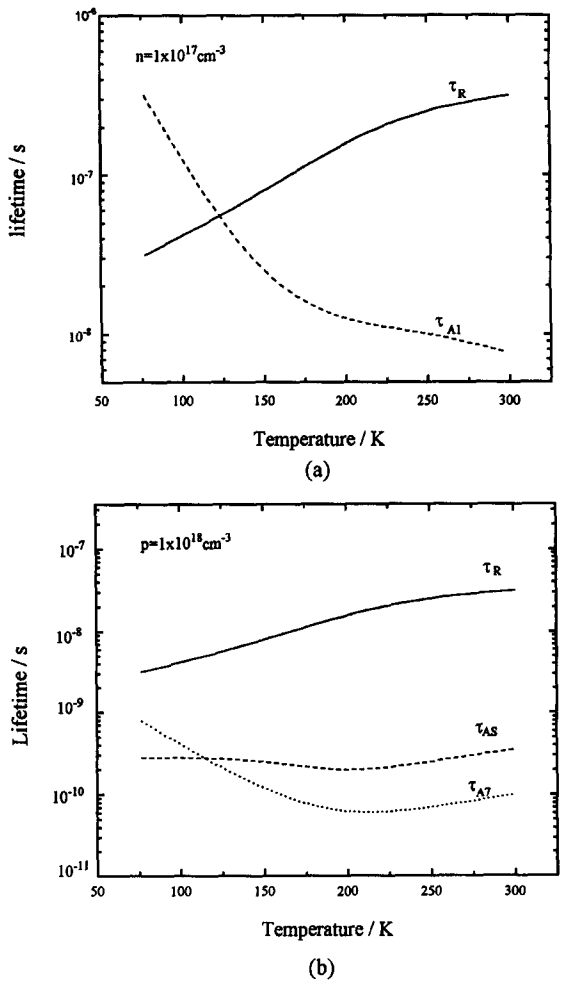

Fig. 7. Dependence of minority-carrier lifetimes on temperature for (a) n-type ($n = 1 \times 10^{17}$ cm^{-3}) and (b) p-type ($p = 1 \times 10^{18} cm^{-3}$) $InAs_{0.90}Sb_{0.10}$.

Comparison of the calculated and experimental internal quantum efficiency (η_{int}) for the $InAs_{0.91}Sb_{0.09}$ epitaxial layers and LEDs are listed in Table 1. The calculated minority-carrier lifetimes of radiative and Auger recombination for the n- and p-type $InAs_{0.91}Sb_{0.09}$ epitaxial layers are shown in Fig. 7. The experimentally measured quantum efficiencies at 77 K and room temperature measured from the LEDs are in good agreement with the theoretical values obtained for the p-region, and are apparently ($\sim 10\times$) lower than the theoretical value for the i-layer. This is because the actual active layer in these n–i–p/P LEDs is the p-layer not the i-layer just as discussed earlier.

It is therefore reasonably expected that the quantum efficiency of these LEDs could be increased further if recombination could be forced to occur in the i-layer by improving the design of the LED. However, the quantum efficiency has apparently reached the theoretical limit in our p-type material, imposed by Auger recombination.

4. Conclusion

High quality $InAs_{0.90}Sb_{0.10}$ epitaxial material grown on GaSb substrates by liquid phase epitaxy was fabricated into n–i–p-$InAs_{0.91}Sb_{0.09}$/P-GaSb LEDs. Strong electroluminescence at room temperature was obtained with the emission spectrum peaking at 4.2 μm. The output power of the n–i–p/P diodes made in this work was measured to be 2.9 μW at 300 K and the external quantum efficiency was 10^{-4} at room temperature. It is anticipated that these uncooled devices are suitable as sources for use in a CO_2 detection instrument which could be used in various applications.

References

[1] Woolly and J. Warner, Can. J. Phys. 42 (1964) 879.
[2] M.P. Mikhailova and A.N. Titkov, Semicond. Sci. Technol. 9 (1994) 1279.
[3] N.P. Esina, N.V. Zotova, I.I. Markov, B.A. Matveev, A.A. Rogachev, N.M. Stus and G.N. Talalakin, J. Appl. Spectrosc. 42 (1985) 465.
[4] Y. Mao and A. Krier, J. Crystal Growth 133 (1993) 108.

[5] H. Mani, A. Joullie, J. Bhan, C. Schiller and J. Primot, J. Electron. Mater. 16 (1987) 289.
[6] J.L. Zyskind, A.K. Srivastava, J.C. DeWinter, M.A. Pollack and J.W. Sulhoff, J. Appl. Phys. 61 (1987) 2898.
[7] J.R. Skelton and J.R. Knight, Solid-State Electron. 28 (1985) 1166.
[8] S.B. Bondar, V.N. Vigdorovich, G.P. Furmanov and S.G. Shutov, Sov. Phys. Tech. Phys. 27 (1982) 215.
[9] L.O. Bubulac, A.M. Andrews, E.R. Gertner and D.T. Cheung, Appl. Phys. Lett. 36 (1980) 734.
[10] E.R. Gertner, A.M. Andrews, L.O. Bubulac, D.T. Cheung, M.J. Ludowise and R.A. Riedel, J. Electron. Mater. 8 (1979) 545.
[11] A.M. Andrews, D.T. Cheung, E.R. Gertner and J.T. Longo, J. Vac. Sci. Technol. 13 (1976) 961.
[12] G.B. Stringfellow and P.E. Greene, J. Electromchem. Soc. 118 (1971) 805.
[13] S. Elies, A. Krier, I.R. Cleverley and K. Singer, J. Phys. D 26 (1993) 159.
[14] J. DeBoeck, W. Dobbelaere, J. Vanhellement, R. Mertens and G. Borghs, Appl. Phys. Lett. 58 (1991) 928.
[15] W. Dobbelaere, J. DeBoeck and G. Borghs, Appl. Phys. Lett. 55 (1989) 1856.
[16] T.Y. Seong, A.G. Morman, G.R. Booker, R. Droopad, R.L. Williams, S.D. Parker, P.D. Wang and R.A. Stradling, Mater. Res. Soc. Symp. Proc. 163 (1989) 907.
[17] M.Y. Yen, R. People and K.W. Wecht, J. Appl. Phys. 64 (1988) 952.
[18] M.Y. Yen, R. People and K.W. Wecht and A.Y. Cho, Appl. Phys. Lett. 52 (1988) 489.
[19] M.Y. Yen, B.F. Levine, C.G. Bethea, K.K. Choi and A.Y. Cho, Appl. Phys. Lett. 50 (1987) 927.
[20] J.I. Chyi, S. Kalem, N.S. Kumar, C.W. Litton and H. Morkock, Appl. Phys. Lett. 53 (1988) 1092.
[21] G.S. Lee, Y. Lo, Y.F. Lin, S.M. Bedair and W.D. Laidig, Appl. Phys. Lett. 50 (1985) 1219.
[22] T.H. Chiu, W.T. Tsang, J.A. Ditzenberger, S.N.G. Chu and J.P. Ven der Ziel, J. Appl. Phys. 60 (1986) 205.
[23] J.P. Ven der Ziel, T.H. Chiu and W.T. Tsang, Appl. Phys. Lett. 47 (1985) 1139.
[24] T. Tang, T.H. Chiu, D.W. Kisker and J.A. Ditzenberger, Appl. Phys. Lett. 46 (1985) 283.
[25] Z.M. Fang, K.Y. Ma, D.H. Jaw, R.M. Cohen and G.B. Stringfellow, J. Appl. Phys. 67 (1990) 7034.
[26] P.K. Chiang and S.M. Bedair, J. Electrochem. Soc. 131 (1984) 2422.
[27] C. Besikci, Y.H. Choi, G. Labeyrie, E. Bigan and M. Razeghi, J. Appl. Phys. 76 (1994) 5820.
[28] Y. Mao and A. Krier, J. Electron. Mater. 23 (1994) 503.
[29] Y. Mao and A. Krier, J. Phys. Chem. Solids 56 (1995) 759.
[30] H.Q. Le, G.W. Turner, S.J. Eglash, H.K. Choi and D.A. Coppeta, Appl. Phys. Lett. 62 (1984) 152.
[31] W. Dobbelaere, J. De Boeck, C. Brynseraede, R. Mertens and G. Borghs, Electron. Lett. 29 (1993) 890.
[32] D.T. Cheung, A.M. Andrews, E.R. Gertner, G.M. Williams, J.E. Clarke, J.G. Pasko and J.T. Longo, Appl. Phys. Lett. 30 (1977) 587.
[33] A. Krier and Y. Mao, Semicond. Sci. Technol. 10 (1995) 930.
[34] S. Tsukamoto, P. Bhattacharya, Y.C. Chen and J.H. Kim, J. Appl. Phys. 67 (1990) 6819.
[35] A. Rogalski and Z. Orman, Infrared Phys. 25 (1985) 551.
[36] A. Sugimura, IEEE J. Quantum. Electron. QE-18 (1982) 352.
[37] H.H. Wieder, Appl. Phys. Lett. 25 (1974) 206.
[38] T.S. Moss, Handbook on Semiconductors, Vol. 4 (North-Holand, Amsterdam, 1993).
[39] J. Wilson and J.F.B. Hawkes, Optoelectronics: An Introduction, 2nd ed. (Prentice-Hall, Englewood Cliffs, NJ, 1989).